# Maximum Output Power Tracking Control in Variable-Speed Wind Turbine Systems Considering Rotor Inertial Power

Kyung-Hyun Kim, Tan Luong Van, *Student Member, IEEE*, Dong-Choon Lee, *Member, IEEE*, Seung-Ho Song, *Member, IEEE*, and Eel-Hwan Kim, *Member, IEEE*

*Abstract*—**This paper proposes a new maximum power point tracking (MPPT) algorithm for variable-speed wind turbine systems, which takes advantage of the rotor inertia power. In this method, a proportional controller is added to the power control to effectively reduce the moment of inertia of the wind turbines, which can improve the fast performance of the MPPT control. The PSIM simulation and experimental results for a doubly-fed induction generator wind turbine system have proved the validity of the proposed algorithm.**

*Index Terms*—**Inertia, maximum power point tracking (MPPT), power control, torque control, wind turbine.**

## I. Introduction

RECENTLY, variable-speed wind turbine systems have been being installed in field applications. Compared with the fixed-speed types, the variable-speed wind turbine systems have a wide speed range of operation and provide 10%–15% higher energy capture from the wind turbine [1].

The control method to capture the maximum power from wind turbines in the variable-speed region is called tracking (MPPT) control. The MPPT control is accomplished by tracking the maximum power coefficient ($C_{p\max}$) locus on the wind turbine characteristic curve below the rated rotational speed. There are four categories of the MPPT methods in the wind turbine system: power signal feedback (PSF) control, perturbation and observation (P&O) control, tip-speed ratio (TSR) control, and optimal torque control [2], [3].

The PSF controller based on the maximum power curve of the wind turbine needs the rotor speed for yielding the corresponding power reference [4], [5]. The maximum output power characteristics resulting from the simulation and field tests are stored in a form of lookup table in the memory. Once the lookup table is programmed, it is easy to implement the MPPT control without the need of the wind speed measurement. In addition, this method is rather stable since the data in the lookup table are obtained by the real test. However, it is difficult to get the field data.

The P&O method normally needs the rotor speed and the turbine power variation for the MPPT. The advantage of the P&O method is that it requires neither turbine characteristic curve nor generator parameters [6]. It makes the control algorithm robust even though the parameter varies. However, the P&O method is inappropriate in large-inertia wind turbine systems since the generator power is influenced by the turbine power and the change rate of the rotor inertial energy, which often renders the P&O method inefficient. Thus, a tradeoff is needed between the convergence time and the accuracy for the MPPT control.

The TSR control regulates the rotational speed to keep the optimal TSR. The advantage of this method is a simple implementation; however, the wind speed information should be provided. The performance of the TSR control depends on the anemometer accuracy [7]. Alternatively, an estimated wind speed can be utilized for this method [8].

In the conventional optimal torque control method, the generator torque is controlled to its optimal value corresponding to the maximum power conversion coefficient ($C_{p\max}$) [9]. In this method, the torque reference is proportional to the square of the rotor speed, and the output power is proportional to the cube of the rotor speed. Since the rotor speed variation is relatively low in the megawatt-class wind turbines, the width of the generator power variation is also narrow. The shortcoming of the optimal torque control is the slow response time for wind speed variations.

The aforementioned MPPT methods are based on the steady-state characteristics where the effect of the turbine inertia is neglected. A few algorithms have been proposed to consider the rotor inertia for the MPPT control. In [1], the optimal operating points of the wind turbine can be reached through the intelligent memory which is obtained by the online training process. This method needs no measurements of the wind speed
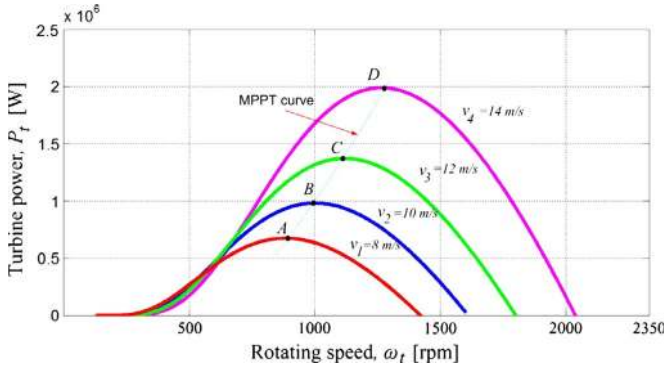
Fig. 1.   $P_t$–$\omega_t$ curve ($\beta = 0°$).

and the rotor speed. However, it requires a training process with a large amount of memory. In [2], the rotor inertia effect has been included for the fast MPPT control. However, its implementation is complex since the turbine torque observer is needed. In [10], a relationship between the energy capture and drivetrain torque transient has been investigated. When the $C_p$ becomes sharper and the rotor inertia decreases, the energy production is increased, and the power ripples into the grid are also increased. However, any quantitative analysis has not been provided in detail. In [3], a new method has been proposed by the authors for the fast MPPT performance, in which the large inertia effect of the wind turbine was investigated. A proportional control loop is added to the torque control to reduce the effect of the moment of inertia in the wind turbines.

In this paper, a new power controller is proposed for the MPPT control, which is less sensitive to the machine parameters than the torque control method. To verify the effectiveness of the proposed algorithm, the simulation results for the 2-MW doubly fed induction generator (DFIG) wind turbine system are provided. Also, experimental results are presented for the 3-kW laboratory-scale wind turbine simulator.

This paper is organized as follows. The modeling of the wind turbine systems is described in Section II. Next, the optimal torque control for the MPPT is described in Section III. Then, the proposed MPPT method is analyzed in Section IV. The simulation and experimental results for the DFIG wind turbine system are investigated in Sections V and VI, respectively.

## II. MODELING OF WIND TURBINE SYSTEMS

### A. Modeling of Wind Turbines

The output power of wind turbines ($P_t$) is determined as [11], [12]

$$P_t = \frac{1}{2}\rho\pi R^2 C_p(\lambda, \beta)V^3 \qquad (1)$$

where $\rho$ is the air density (in kilograms per cubic meter), $R$ is the radius of the blade (in meters), $V$ is the wind speed (in meters per second), and $C_p(\lambda, \beta)$ is the power conversion coefficient which is a function of the TSR ($\lambda$) and the pitch angle ($\beta$). The wind turbine is characterized by ($P_t$–$\omega_t$) curves, as shown in Fig. 1.

The TSR $\lambda$ is defined as [13]

$$\lambda = \frac{R\omega_t}{V} \qquad (2)$$

where $\omega_t$ is the rotor speed of turbines. The power conversion coefficient is expressed as follows:

$$C_p(\lambda, \beta) = c_1\left(c_2\frac{1}{\Lambda} - c_3\beta - c_4\beta^{c_5} - c_6\right)\exp\left(-c_7\frac{1}{\Lambda}\right) \qquad (3)$$

where

$$\frac{1}{\Lambda} = \frac{1}{\lambda + 0.08\beta} - \frac{0.035}{1 + \beta^3} \qquad (4)$$

and $c_1$–$c_7$ are the constants [14]–[16].

From (1) and (2), the turbine torque can be expressed as

$$T_t = \frac{1}{2}\rho\pi R^3 \frac{C_p(\lambda, \beta)}{\lambda}V^2. \qquad (5)$$

### B. Linearization of Wind Turbine Aerodynamics

The turbine torque with one-mass modeling of wind turbine systems is expressed as [16]–[18]

$$T_t = J_t\frac{d\omega_t}{dt} + B_t\omega_t + T_g \qquad (6)$$

where $J_t$ is the combined inertia of the turbine and generator, $B_t$ is the damping coefficient of the turbine, and $T_g$ is the generator torque. For the small-signal analysis, applying a small perturbation at the operating point ($\omega_{to}, \beta_o, V_o$) to the turbine torque in (6)

$$(T_{to}+\delta T_t) = J_t\frac{d(\omega_{to}+\delta\omega_t)}{dt} + B_t(\omega_{to}+\delta\omega_t) + (T_{go}+\delta T_g). \qquad (7)$$

As well known, the turbine torque is a function of the wind speed, the rotational speed, and the pitch angle. Taking the partial derivative from the turbine torque in (6) [11], [16], [19]

$$\delta T_t = -B_r \cdot \delta\omega_t + k_{r,\beta} \cdot \delta\beta + k_{r,V} \cdot \delta V \qquad (8)$$

where

$$B_r = -\left.\frac{\partial T_t}{\partial\omega_t}\right|_{(\omega_{t0},\beta_0,V_0)}, \qquad k_{r,\beta} = \left.\frac{\partial T_t}{\partial\beta}\right|_{(\omega_{t0},\beta_0,V_0)}$$

$$k_{r,V} = \left.\frac{\partial T_t}{\partial V}\right|_{(\omega_{t0},\beta_0,V_0)}, \qquad T_{t0} = T_t|_{(\omega_{t0},\beta_0,V_0)}.$$

$B_r$ is the intrinsic speed feedback of the turbine, $k_{r,V}$ denotes the gain between the wind speed and the turbine torque, and $k_{r,\beta}$ is the gain between the pitch angle and the turbine torque. The gains ($B_r$, $k_{r,V}$, and $k_{r,\beta}$) of typical variable-speed variable-pitch wind turbine systems are shown in Fig. 2, which are variable and updated at every operating point of the system. The $k_{r,\beta}$ and $B_r$ vary a little at low wind speeds and relatively much at high wind speeds. However, in the case of the $k_{r,V}$, it is reverse.
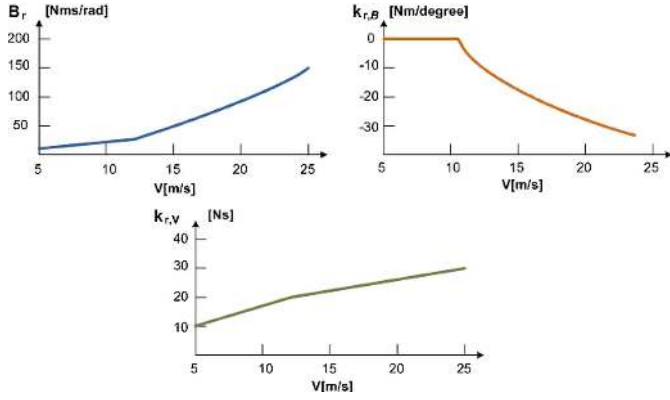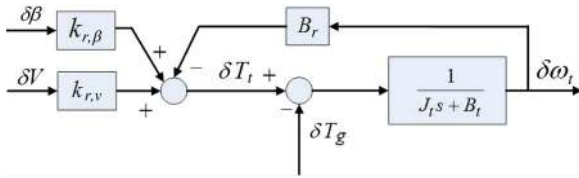
Fig. 2. Gains of a turbine torque.



Fig. 3. Linearized turbine model.

From (7) and (8), the mechanical torque is rewritten as

$$J_t \frac{d\delta\omega_t}{dt} + (B_t + B_r)\delta\omega_t = K_{r,\beta}\delta\beta - \delta T_g + K_{r,V}\delta V. \quad (9)$$

The turbine model linearized at the operating point in (9) is shown in Fig. 3.

In the case that the gain $k_{r,\beta}$ is ignored since the pitch angle control is not used for the MPPT, the values of $B_r$ and $k_{r,V}$ are updated at every operating point of the system from (8), which are used for the modeling of the wind turbine in the block diagrams in Figs. 6, 7, and 10.

### C. DFIG Wind Generation System

Fig. 4 shows a circuit configuration and control block diagram of a DFIG wind power system. The DFIG circuit configuration is composed of a wound rotor induction generator whose stator and rotor are directly connected to the grid and interfaced through the back-to-back converters, respectively. Two vector control schemes in the synchronous reference frames are used for the grid-side converter (GSC) and the rotor-side converter (RSC) of DFIG wind turbine systems [13], [20]–[23]. The control structure of the GSC is composed of the outer dc-link voltage control loop and the inner current control loops. The purpose of the control scheme is to keep the dc-link voltage constant and to control the grid reactive power to be zero. With the RSC, the vector control scheme for the DFIG control consists of the outer control loops of the stator active and reactive powers and the inner current control loops. The reactive power reference is normally set to zero for the RSC to get the unity power factor at the stator terminal. Several methods have been proposed for the MPPT control of the DFIG [24], [25]. The conventional torque control scheme will be described in the next section.

## III. OPTIMAL TORQUE CONTROL FOR MPPT

### A. Principle of MPPT

In order to obtain the maximum output power from the wind speed, the turbine should operate at the optimal TSR. The relation between the torque and the rotor speed is expressed in Newton's law of motion as [23], [25]

$$T_t - T_g = T_J = J_t \frac{d\omega_t}{dt} + B_t\omega_t \quad (10)$$

where $T_J$ represents the inertial torque of the rotor.

The relation between the turbine and generator torques is shown in Fig. 5. If the wind speed changes from $V_1$ to $V_2$, the turbine torque at point B becomes larger than the generator torque. Thus, the turbine is accelerated up to point C which is a new operating point. There are a lot of paths to reach the new MPP when the wind speed varies.

### B. Optimal Torque Control

According to (10), the optimal torque control scheme forces the generator to follow the locus of $C_{p\,\max}$ continuously when the wind speed changes. As a result, the rotor speed moves to the new equilibrium point. Fig. 6 shows the block diagram of optimal torque control. When the wind speed is below the rated value, the pitch angle controller is deactivated.

For the optimal TSR, the turbine speed should be changed according to the wind speed. The maximum turbine power $(P_{t\_\max})$ is expressed with the corresponding rotor speed $(\omega_{\mathrm{opt}})$ as [13]

$$P_{t\_\max} = K_{\mathrm{opt}}\omega_{\mathrm{opt}}^3 \quad (11)$$

where $K_{\mathrm{opt}} = 0.5\rho\pi R^5 C_{p\,\max}(1/\lambda_{\mathrm{opt}})^3$.

Then, the generator torque reference from the rotational speed is expressed as

$$T_g^* = K_{\mathrm{opt}}\omega_t^2. \quad (12)$$

In the optimal torque control, the torque reference of the DFIG can be linearized at the operating point, which is expressed as [3]

$$\begin{aligned} T_g^*(= T_g) &= T_{g0} + \delta T_g \\ &= K_{\mathrm{opt}}(\omega_{to} + \delta\omega_t)^2 \\ &\approx K_{\mathrm{opt}}\omega_{to}^2 + 2K_{\mathrm{opt}}\omega_{to}\delta\omega_t \end{aligned} \quad (13)$$

where $\omega_{t0}$ is the rotor speed at the operating point.

From Fig. 6, the transfer function between the turbine torque and the rotor speed is derived as [3]

$$G(s) = \frac{\delta\omega_t}{\delta T_t} = \frac{1}{J_t s + B_t + B_r + 2K_{\mathrm{opt}}\omega_{to}}. \quad (14)$$

The torque of the DFIG is directly proportional to the current, so the torque dynamics is assumed to be negligible since the time constant in the electrical system is much shorter than that of the mechanical system.
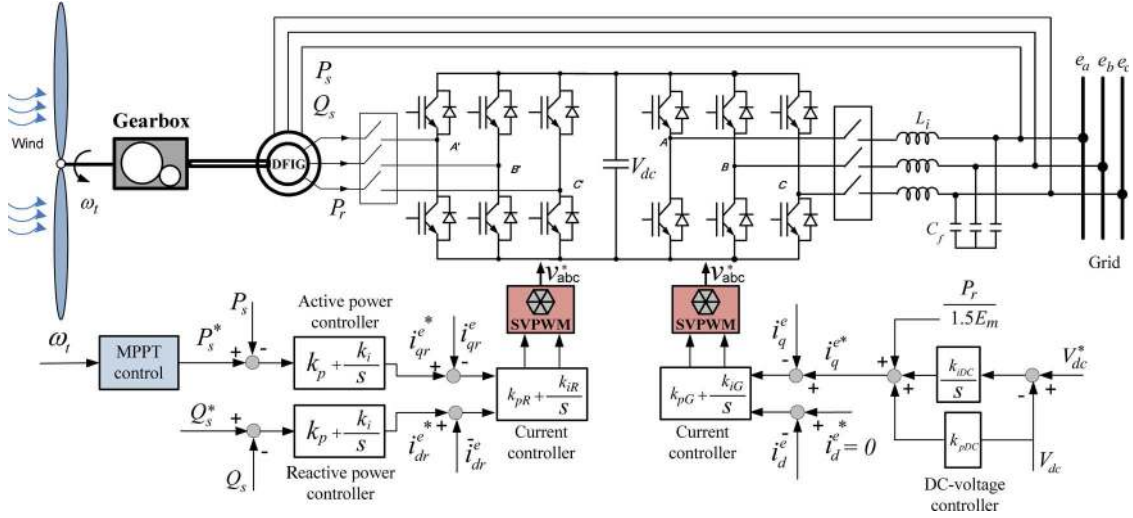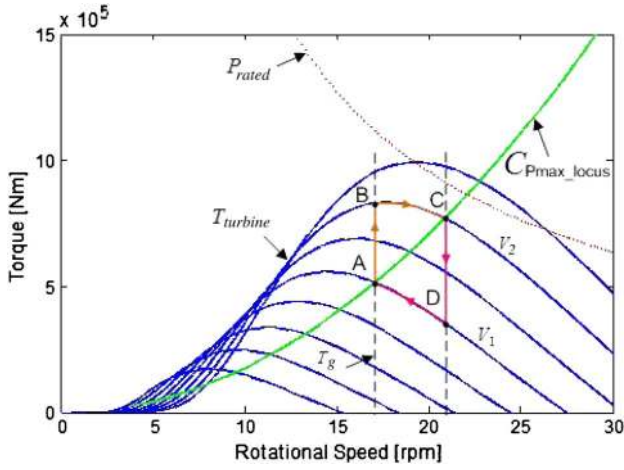
Fig. 4.  DFIG wind power generation system.



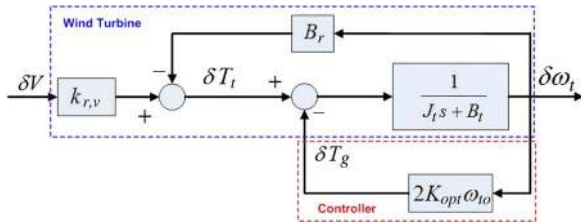Fig. 5.  Turbine torque in torque–rotational-speed plane.



Fig. 6.  Model of wind turbine system including the optimal torque control.

## IV. PROPOSED MPPT CONTROL

### A. Proposed Torque Control

As the wind speed varies, the dynamic response in the optimal torque control is restricted since the torque reference is determined by the rotor speed. In order to improve the performance of the MPPT control in the transient state, the difference between the turbine torque and the generator torque needs to be large, which leads to the fast acceleration or deceleration of the system. In addition, the MPPT control method has to keep the $C_p$ at the maximum value at the steady state. To satisfy this requirement, a proportional controller is added to the optimal torque controller. Then, Fig. 6 is modified to Fig. 7. From
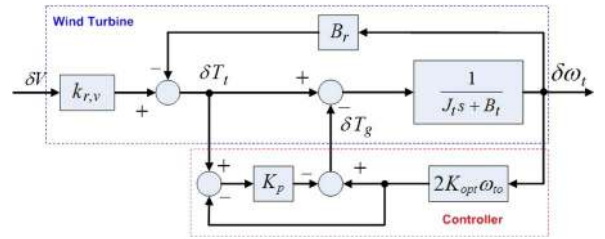


Fig. 7.  Model of wind turbine system including the proposed torque control.

this model, the generator torque reference is calculated for the MPPT control.

This controller is effective only in the transient state, and its effect disappears in the steady state where the proposed controller has the same characteristics as the optimal torque one described in the last section.

With the proportional control loop, the transfer function in (14) is modified as

$$G'(s) = \frac{\delta\omega_t}{\delta T_t} = \frac{1}{\frac{J_t}{(1+K_p)}s + \frac{B_t}{(1+K_p)} + B_r + 2K_{opt}\omega_{to}}$$

$$= \frac{1}{J'_t s + B'_t + B_r + 2K_{opt}\omega_{to}} \qquad (15)$$

where

$$J'_t = \frac{J_t}{(1+K_p)} \qquad B'_t = \frac{B_t}{(1+K_p)} \qquad (16)$$

and $K_p$ is a proportional gain. The transient performance of the MPPT control depends on this proportional gain.

It is noticed from (16) that the moment of inertia $(J'_t)$ and the damping coefficient $(B'_t)$ are effectively reduced by the proportional gain, which makes the dynamic response faster. Thus, a large-inertia wind turbine system can be controlled similarly to a small-scale one under the torque capability of the system. However, since the practical wind turbine system has physical limitations, the proportional gain should be selected carefully. In this research, the gains are empirically selected by trial and error, which are 0.9 and 2.2 for the simulation and experiment, respectively.
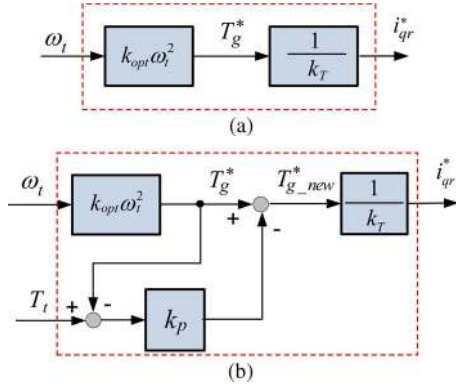
Fig. 8. MPPT control block diagram. (a) Optimal torque control. (b) Proposed torque control.
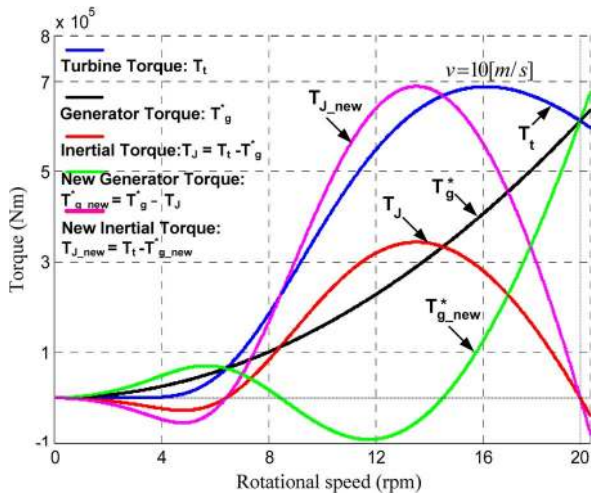


Fig. 9. Effect of inertia on the turbine system with and without an additional proportional gain.

Fig. 8(a) and (b) shows the MPPT control block diagrams for the optimal torque control method and the proposed torque control method, respectively. The torque reference divided by the torque constant $(k_t)$ commands the rotor $q$-axis current reference. This MPPT control block diagram can be substituted into the corresponding part in Fig. 4.

Fig. 9 shows the effect of the inertia on the turbine system according to the rotational speed, at the wind speed of 10 m/s, with or without an additional proportional control loop, where the optimal $\lambda$ is 7.952, corresponding to the $C_{p\max}$ of 0.411.

For the conventional optimal torque control method, the difference between the turbine and generator torques $T_t - T_g^*$ determines an inertial torque $T_J$, which accelerates or decelerates the turbine system.

It is noted that the electrical power varies more quickly than the mechanical one due to the turbine and generator inertia. If a large inertia is considered, any change in the turbine speed will cause a large variation in the generator power. Then, the kinetic energy is absorbed or released so slowly that the MPPT performance becomes sluggish.

To overcome this drawback, a proportional controller is introduced to reduce the effects of the moment of inertia and the damping coefficient. With the proposed torque control method, of which the block diagram is shown in Fig. 8(b), if the $k_p$

is temporarily assumed to be one for easy explanation, the generator torque reference is decreased to $T_{g\_new}^*$. Then, the inertial torque is increased to $T_{J\_new}$, so that the turbine can accelerate faster. When the wind speed decreases, the inertial torque becomes more negative.

As can be seen from Fig. 9, an inertial torque in the proposed method is larger than that in the optimal torque control method. Thus, the acceleration of the rotor will be faster.

### B. Proposed Power Control

The machine parameters are usually needed in calculating the generator torque. To avoid the dependence of the torque controller on the machine parameters, a power controller can be adopted, where the power is calculated from the measured voltages (actually, voltage references) and currents without using any machine parameter.

In the case of a small disturbance, the turbine power at an operating point $(\omega_{to}, \beta_o, V_o)$ is expressed as

$$P_t = \omega_t \cdot T_t = (\omega_{to} + \delta\omega_t)(T_{to} + \delta T_t) = P_{to} + \delta P_t$$
$$= \frac{1}{2} J_t \frac{d(\omega_{to} + \delta\omega_t)^2}{dt} + B_t(\omega_{to} + \delta\omega_t)^2$$
$$+ P_{go} + \delta P_g. \tag{17}$$

For the MPPT control, the generator power reference is obtained from (11) as

$$P_g^* = K_{\mathrm{opt}} \cdot \omega_t^3. \tag{18}$$

In the case of a small disturbance, the generator power at the operating point $(\omega_{to}, \beta_o, V_o)$ can also be expressed as

$$P_g^* = P_g = P_{go} + \delta P_g = \omega_t \cdot T_g$$
$$= (\omega_{to} + \delta\omega_t)(T_{go} + \delta T_g) = K_{\mathrm{opt}}(\omega_{to} + \delta\omega_t)^3. \tag{19}$$

From (19), the $\delta P_g$ is approximated as

$$\delta P_g \approx T_{go}\delta\omega_t + \omega_{to}\delta T_g \approx 3K_{\mathrm{opt}}\omega_{to}^2\delta\omega_t. \tag{20}$$

According to (17), the turbine power is expressed as

$$\delta P_t = \omega_{to}\delta T_t = \omega_{to}J_t\frac{d(\delta\omega_t)}{dt} + B_t\omega_{to}\delta\omega_t + 2K_{\mathrm{opt}}\omega_{to}^2\delta\omega_t. \tag{21}$$

Similar to the proposed torque control, the proportional controller in the power control method can also improve the dynamics of the rotational speed. The linearized model of wind turbines including the proposed power control is shown in Fig. 10. This model is used to calculate the generator power reference for the MPPT control.

The transfer function describing the relation of the turbine power and the rotational speed is given by

$$G(s)'' = \frac{\delta\omega_t}{\delta P_t} = \frac{1}{\frac{J_t}{(1+K_p)}s + \frac{B_t}{(1+K_p)} + B_r + 2K_{\mathrm{opt}}\omega_{to}^2}$$
$$= \frac{1}{J_t's + B_t' + B_r + 2K_{\mathrm{opt}}\omega_{to}^2} \tag{22}$$
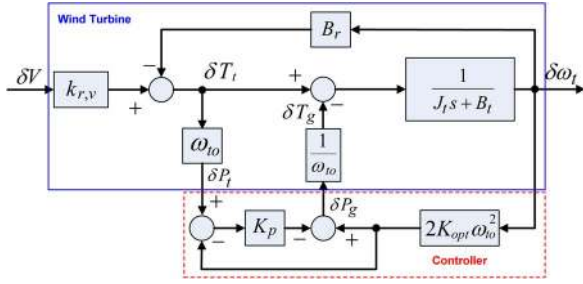
Fig. 10.   Model of wind turbine system including the proposed power control.
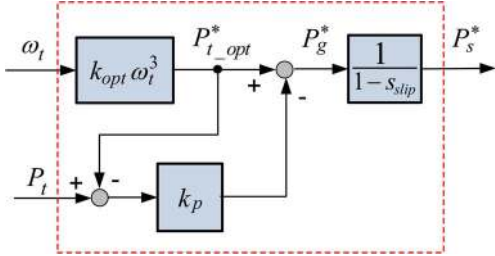


Fig. 11.   Block diagram of proposed power control.

which is similar to (15). With the $K_p$ positive, the equivalent moment of inertia $J_t'$ can be reduced. Thus, the dynamic response will be faster.

Fig. 11 shows the block diagram of the proposed power control method, which includes a simple proportional control loop. The stator power reference is obtained by dividing $P_g^*$ by $(1 - s_{\text{slip}})$, where $s_{\text{slip}}$ denotes the slip of the machine.

This MPPT control block diagram can be substituted into the corresponding part in Fig. 4. For our control, the wind speed is not needed. Instead, the generator speed is required. The complex transfer function has been derived to express the dynamic behavior of the wind turbine system. For actual implementation, the aforementioned MPPT control block is employed.

## V. SIMULATION STUDIES

To verify the effectiveness of the proposed method (power controller), the simulation has been carried out using the PSIM software. The system parameters for the wind turbine and the DFIG are shown in Tables I and II, respectively. In this work, a stepwise-varying wind speed and a randomly varying wind speed are considered for the simulation condition. Also, the damping coefficient is ignored in the simulation.

### A. Stepwise Wind Speed Changes

Figs. 12 and 13 show the dynamic responses of the optimal torque control and the proposed power control methods, respectively, when the wind speed changes from 7 to 9 m/s at 40 s and back to 7 m/s at 70 s. Fig. 12(b) shows the power conversion coefficient, where the $C_p$ is recovered to $C_{p\max}$ in 17 s after the sudden drop at 40 s. Meanwhile, it takes just 5 s for the proposed power control method.
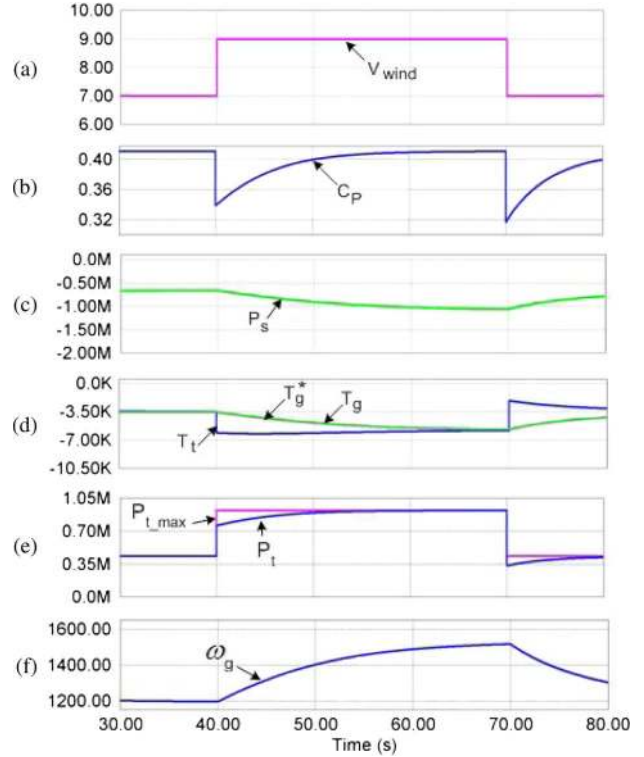


Fig. 12.   Responses of optimal torque control in stepwise wind speed variation. (a) Wind speed. (b) Power conversion coefficient. (c) Stator active power. (d) Turbine torque, generator torque, and generator torque reference. (e) Actual and maximum available turbine powers. (f) Generator speed.

Compared with the optimal torque control method, the $C_p$ variation gives faster response during the stepwise change of the wind speed. As can be seen in Fig. 12(c), the stator active power is also varied, and then, it reaches the steady state after 17 s. However, in the case of the proposed power control method as shown in Fig. 13(c), this value not only follows its reference well but also shows faster performance than that of the optimal torque control method.

The generator torque reference, the actual generator torque, and the turbine torque are shown in Fig. 12(d). With the conventional method, the generator torque follows its reference value and reaches the steady state after 19 s. However, with the proposed method, the response generator torque, as shown in Fig. 13(d), becomes better when compared with the conventional one. Also, the actual turbine power $(P_t)$ in the proposed method, as shown in Fig. 13(e), reaches the maximum value $(P_{t\_\max})$ faster than that in the conventional control one [Fig. 12(e)]. With the same wind speed variation, the generator speed in both cases is increased. However, the generator speed [Fig. 13(f)] in the proposed method accelerates more rapidly than it does in the optimal torque control one [Fig. 12(f)]. As a result, more turbine power can be captured.

The power control method provides better performance than the optimal torque control one in transient state due to the proportional controller. It should be noted that the stator active power reference in the proposed method is limited to zero, as shown in Fig. 13(c), to prevent the generator from operating in a motoring mode in transient state.
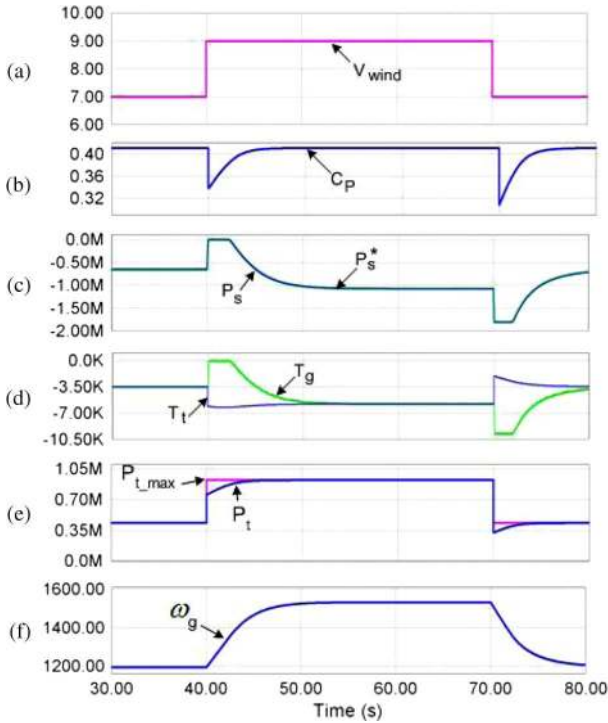
Fig. 13. Responses of proposed power control in stepwise wind speed variation. (a) Wind speed. (b) Power conversion coefficient. (c) Stator active power. (d) Turbine torque and generator torque. (e) Actual and maximum available turbine powers. (f) Generator speed.

## B. Randomly Varying Wind Speed

The simulation has been performed in the condition of random changes of the wind speed. The results of the optimal torque control and proposed power control methods are shown in Figs. 14 and 15, respectively. With the proposed power control, it is seen that the $C_p$ value in Fig. 15(b) is increased. Also, the output power of the wind turbine is larger, as shown in Fig. 15(e), and the generator speed also gives faster response, as shown in Fig. 15(f), compared with the optimal torque control method.

The average generator output power, which is not shown here but is of a similar profile to the turbine power, for the given time duration (25 s) in the proposed method is 1.1% higher than that of the optimal torque control method.

Also, with the same pattern of wind speed, the generator output power is increased by 1.95% and 2.99%, at the mean wind speeds of 9 and 10 m/s, respectively, compared with the energy production in the optimal torque method.

With the conventional method, the stator active power and generator speed are relatively smooth, as shown in Fig. 14(c) and (d), respectively, since the generator speed changes slowly to reach the MPP for the wind speed variations. In the proposed one, however, to achieve the optimal TSR, the generator speed accelerates or decelerates faster due to an additional proportional gain. Thus, the stator active power and generator speed change more rapidly, as shown in Fig. 15(c) and (d), respectively.

Fig. 16 shows the generator output power and energy, at the mean wind speed of 10 m/s with the same wind profile
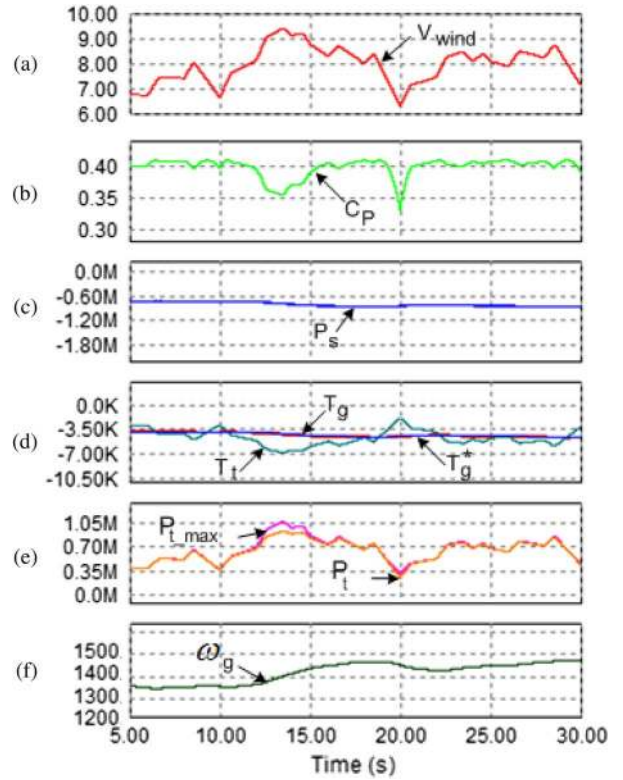


Fig. 14. Responses of optimal torque control in random wind speed variation. (a) Wind speed. (b) Power conversion coefficient. (c) Stator active power. (d) Turbine torque, generator torque, and generator torque reference. (e) Actual and maximum available turbine powers. (f) Generator speed.



Fig. 15. Responses of proposed power control in random wind speed variation. (a) Wind speed. (b) Power conversion coefficient. (c) Stator active power. (d) Turbine torque and generator torque. (e) Actual and maximum available turbine powers. (f) Generator speed.

as Fig. 15(a), for both optimal torque control and proposed power control methods. With the proposed method, the energy production is also 2.99% larger than that of the optimal torque
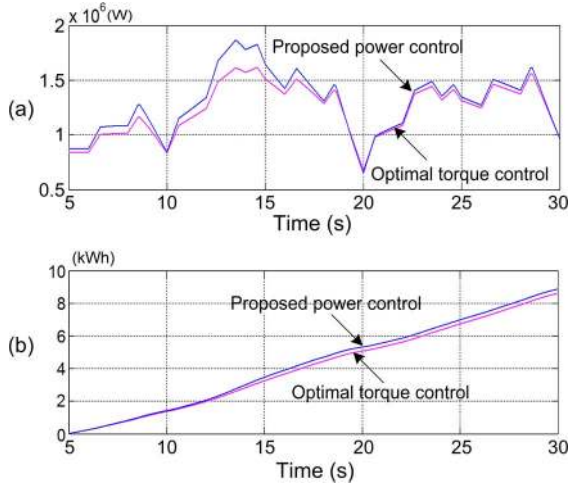
Fig. 16.   Generator output power and energy in a random wind speed variation ($mean = 10$ m/s). (a) Generator output power. (b) Energy.
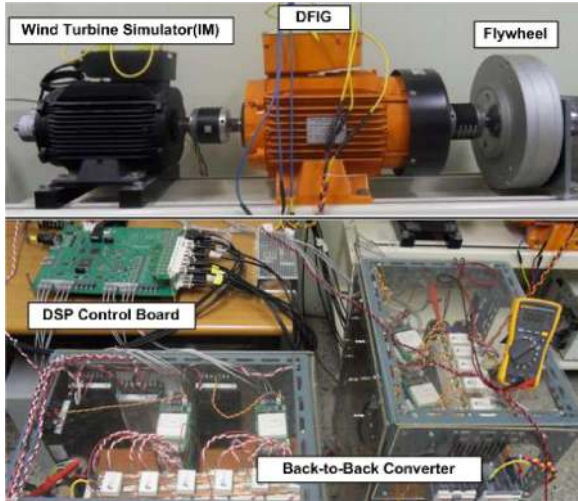


Fig. 17.   Layout of experimental equipment.

control method, for the simulation time duration of 25 s. With the same pattern of wind speed, the energy production is also increased up to about 1.1% and 1.95%, at the mean wind speeds of 8 and 9 m/s, respectively. The higher the mean wind speed, the more the energy production. Of course, the energy production will depend on the wind speed profile, the proportional gain, etc.

## VI. EXPERIMENTAL RESULTS

To demonstrate the validity of the proposed MPPT algorithm, the experiment has been carried out for a 3-kW DFIG wind turbine simulator. The experimental setup at the laboratory is shown in Fig. 17, where a squirrel-cage induction motor is used as a turbine simulator and a flywheel is connected to increase the moment of inertia of the rotor. The parameters of the turbine blade and DFIG are listed in Tables III and IV, respectively.

The GSC controls the dc-link voltage and reactive power whose reference values are 340 V and 0 var, respectively. The capacitance of the dc-link capacitor is 1650 $\mu$F. The switching



Fig. 18.   Responses of optimal torque control in stepwise wind speed variation. (a) Wind speed. (b) Power conversion coefficient. (c) Stator active power. (d) Generator torque and generator torque reference. (e) Turbine torque. (f) Actual and maximum available turbine powers. (g) Generator speed.

frequency is 5 kHz. The rated grid voltage and frequency are 220 $V_{rms}$ and 60 Hz, respectively.

### A. Stepwise Wind Speed Changes

Figs. 18 and 19 show the dynamic responses of the optimal torque control and power control methods, respectively, when the wind speed changes from 6.5 to 9.5 m/s and back to 6.5 m/s [Figs. 18(a) and 19(a)]. The power conversion coefficients for the two methods are shown in Figs. 18(b) and 19(b). It is seen that both of the MPPT control algorithms can reach the MPP successfully. However, the power conversion coefficient values are maintained better in the proposed method.

Thus, the capability of capturing the energy from the wind turbines is improved. With the optimal torque control method, as the wind speed changes, the $C_p$ is recovered to the $C_{p\max}$ in 2 s, as shown in Fig. 18(b). For the proposed method, however, the $C_p$ comes back to the $C_{p\max}$ only in 1 s, as shown in Fig. 19(b).

As can be seen in Fig. 19(c), the stator active power in the proposed power control method is produced more, since it reaches the steady state twice faster than that of the optimal torque control method, as the wind speed changes.

With this optimal torque control method, the generator torque and turbine torque are shown in Fig. 18(d) and (e), respectively. Even though the generator torque in the conventional method follows its reference value, both generator torque and turbine torque do not give the good responses as in the proposed one. Figs. 18(f) and 19(f) show the maximum available and actual turbine powers for the optimal torque control and power control methods, respectively. The actual turbine power in the two cases
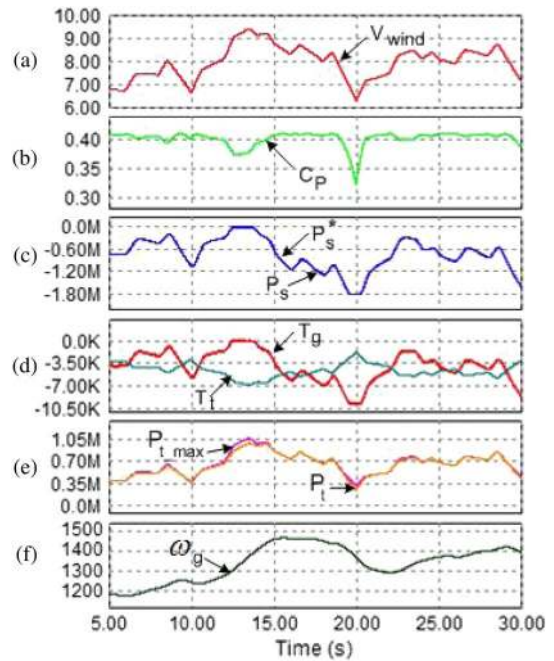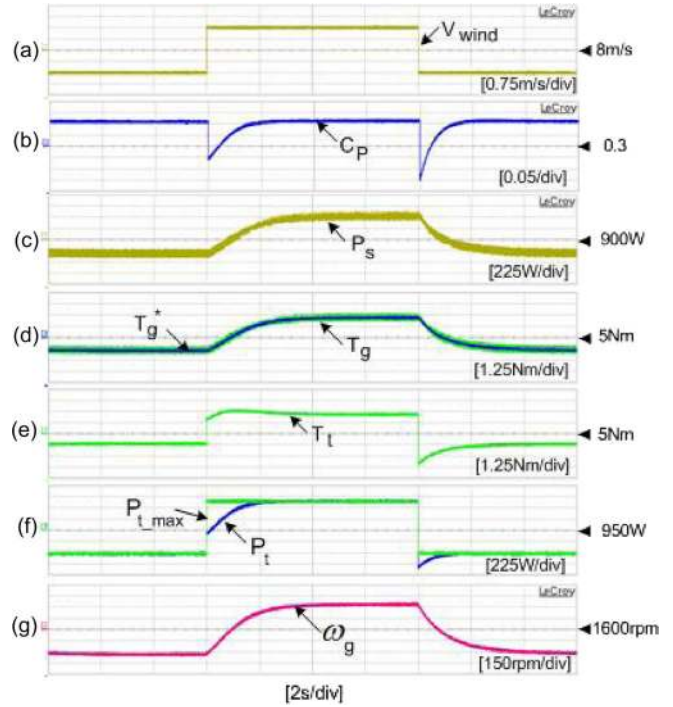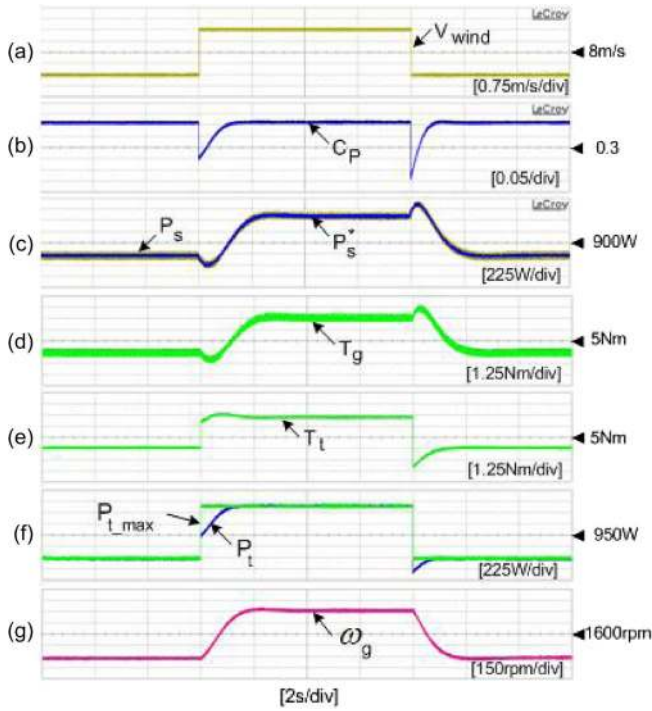
Fig. 19. Responses of proposed power control in stepwise wind speed variation. (a) Wind speed. (b) Power conversion coefficient. (c) Stator active power. (d) Generator torque and generator torque reference. (e) Turbine torque. (f) Actual and maximum available turbine powers. (g) Generator speed.

is controlled to follow the maximum available one. However, the power controller gives the better performance, compared with the torque one. Also, the generator speed in the proposed method gives faster response, as shown in Fig. 19(g). When the wind speed changes, additional stator power reference is produced due to the proportional controller. Thus, it enhances the efficiency of the MPPT control.

### B. Randomly Varying Wind Speed

Figs. 20 and 21 show the MPPT control results of the optimal torque control and power control methods, respectively, when the wind speed varies randomly. Compared with the conventional method, the proposed one gives the better performance to almost all responses. In particular, when comparing Figs. 20(b) and 21(b), the $C_p$ drops up to 0.335 in the proposed method and up to 0.375 in the optimal torque control method. As a result, more stator active power and output power of the wind turbine, as shown in Fig. 21(c) and (f), are also produced.

### VII. CONCLUSION

A new MPPT method for the DFIG wind turbine systems has been proposed, where a proportional controller is added to the power controller to improve the dynamic performance of the MPPT control. Also, the proposed method is robust to the parameter variation of the DFIG since the torque feedback control is not required, different from the conventional optimal torque control scheme. The effect of the proportional gain on the moment of inertia and damping ratio has been analyzed, from which it should be noted that the reduction of these equivalent
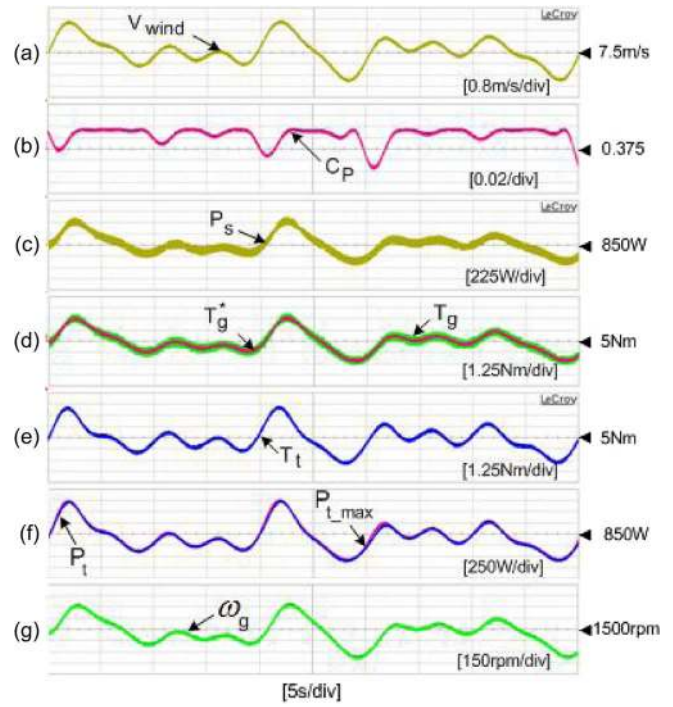


Fig. 20. Responses of optimal torque control in random wind speed variation. (a) Wind speed. (b) Power conversion coefficient. (c) Stator active power. (d) Generator torque and generator torque reference. (e) Turbine torque. (f) Actual and maximum available turbine powers. (g) Generator speed.
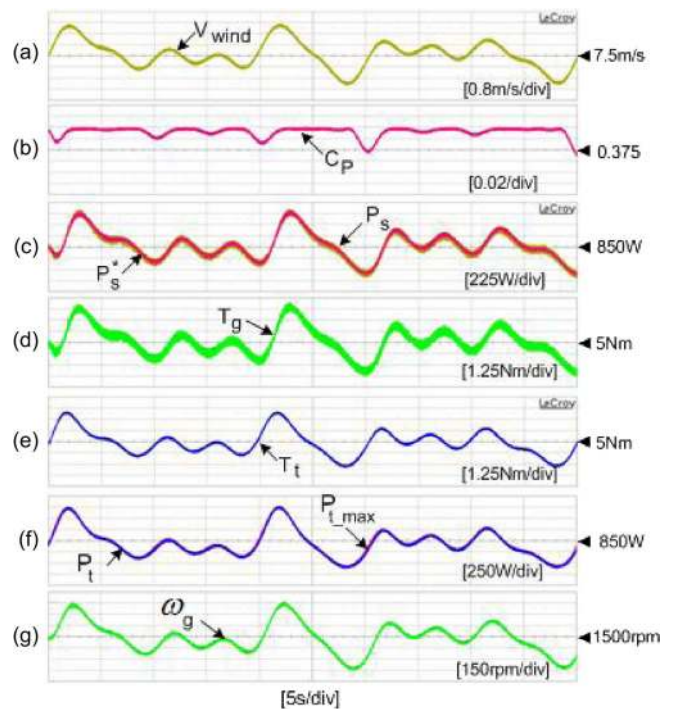


Fig. 21. Responses of proposed power control in random wind speed variation. (a) Wind speed. (b) Power conversion coefficient. (c) Stator active power. (d) Generator torque and generator torque reference. (e) Turbine torque. (f) Actual and maximum available turbine powers. (g) Generator speed.

parameters can yield the faster dynamic performance. On the other hand, the fast MPPT scheme has an effect of mechanical stresses on the wind turbines. Moreover, it will incur the power

TABLE I
PARAMETERS OF WIND TURBINE FOR SIMULATION

| Rated power | 2[MW] |
|---|---|
| Blade radius | 40[m] |
| Air density | 1.225[kg/m$^3$] |
| Max. power conv. coefficient | 0.411 |
| Optimal tip-speed ratio | 7.96 |
| Cut-in speed | 3[m/s] |
| Rated wind speed | 11.65[m/s] |
| Moment of inertia | 5.67x10$^6$[kg.m$^2$] |
| Gear ratio | 90 |

TABLE II
PARAMETERS OF 2-MW DFIG FOR SIMULATION

| Rated power | 2 [MW] |
|---|---|
| Stator voltage/frequency | 690 [V]/60 [Hz] |
| Stator resistance | 0.00488 p.u. |
| Rotor resistance | 0.00549 p.u. |
| Stator leakage inductance | 0.09241 p.u. |
| Rotor leakage inductance | 0.09955 p.u. |
| Generator inertia | 200[kg.m$^2$] |

TABLE III
PARAMETERS OF WIND TURBINE FOR EXPERIMENT

| Rated power | 3 [kW] |
|---|---|
| Air density | 1.225[kg/m$^3$] |
| Blade radius | 1.5[m] |
| Max. power conv. coefficient | 0.411 |
| Optimal tip-speed ratio | 7.96 |
| Gear ratio | 4 |

TABLE IV
PARAMETERS OF 3-kW DFIG FOR EXPERIMENT

| Rated power | 3 [kW] |
|---|---|
| Stator voltage/frequency | 220 [V]/60 [Hz] |
| Stator resistance | 0.0372 p.u. |
| Rotor resistance | 0.04419 p.u. |
| Stator leakage inductance | 0.07737 p.u. |
| Rotor leakage inductance | 1.5592 p.u. |
| Generator inertia | 0.0033[kg.m$^2$] |

pulsation into the grid. Detailed discussion of this issue will be out of the scope of this paper which has investigated the MPPT characteristics of wind turbines. The validity of the control algorithm has been verified by simulation results for a 2-MW DFIG wind power system. Also, the experimental verification has been done for a 3-kW DFIG wind turbine simulator. The experimental results have shown good MPPT control performances under various wind speed conditions.

APPENDIX

This appendix gives the parameters of the wind turbine and generators used for the simulation and experiment (see Tables I–IV).

REFERENCES

[1] Q. Wang and L. Chang, "An intelligent maximum power extraction algorithm for inverter-based variable speed wind turbine systems," *IEEE Trans. Power Electron.*, vol. 19, no. 5, pp. 1242–1249, Sep. 2004.

[2] G. Hua and Y. Geng, "A novel control strategy of MPPT tracking dynamics of wind turbine into account," in *Proc. IEEE Power Electron. Spec. Conf.*, Jun. 2006, pp. 1–6.

[3] K.-H. Kim, D.-C. Lee, and J.-M. Kim, "Fast tracking control for maximum output power in wind turbine systems," in *Proc. AUPEC*, Dec. 2010, pp. 1–5.

[4] M. Ermis, H. B. Ertan, E. Akpinar, and F. Ulgut, "Autonomous wind energy conversion systems with a simple controller for maximum-power transfer," *Proc. Inst. Elect. Eng. B—Elect. Power Appl.*, vol. 139, no. 5, pp. 421–428, Sep. 1992.

[5] S. M. Barakati, M. Kazerani, and J. D. Aplevich, "Maximum power tracking control for a wind turbine system including a matrix converter," *IEEE Trans. Energy Convers.*, vol. 24, no. 3, pp. 705–713, Sep. 2009.

[6] E. Koutroulis and K. Kalaitzakis, "Design of a maximum power tracking system for wind-energy-conversion applications," *IEEE Trans. Ind. Electron.*, vol. 53, no. 2, pp. 486–494, Apr. 2006.

[7] R. Cardenas and R. Pena, "Sensorless vector control of induction machines for variable-speed wind energy applications," *IEEE Trans. Energy Convers.*, vol. 19, no. 1, pp. 196–205, Mar. 2004.

[8] A. G. A. Khalil and D.-C. Lee, "MPPT control of wind generation systems based on estimated wind speed using SVR," *IEEE Trans. Ind. Electron.*, vol. 55, no. 3, pp. 1489–1490, Mar. 2008.

[9] S. Morimoto, H. Nakayama, M. Sanada, and Y. Takeda, "Sensorless output maximization control for variable-speed wind generation system using IPMSG," *IEEE Trans. Ind. Appl.*, vol. 41, no. 1, pp. 60–67, Jan. 2005.

[10] B. Connor and W. E. Leithead, "Investigation of a fundamental trade-off in tracking the $C_{pmax}$ curve of a variable speed wind turbine," in *Proc. 15th BWEA Conf.*, Abingdon, U.K., 1993, pp. 313–319.

[11] F. D. Bianchi, H. D. Battista, and R. J. Mantz, *Wind Turbine Control Systems*. Berlin, Germany: Springer-Verlag, 2007.

[12] B. Singh and S. Sharmay, "Stand-alone wind energy conversion system with an asynchronous generator," *J. Power Electron.*, vol. 10, no. 5, pp. 538–547, Sep. 2010.

[13] V. Akhmatov, *Induction Generators for Wind Power*. Brentwood, U.K.: Multi-Science Publ., 2005.

[14] Z. Lubosny, *Wind Turbine Operation in Electric Power System*. New York: Springer-Verlag, 2003, ch. 5.

[15] M. Pucci and M. Cirrincione, "Neural MPPT control of wind generators with induction machines without speed sensors," *IEEE Trans. Ind. Electron.*, vol. 58, no. 1, pp. 37–47, Jan. 2011.

[16] E. B. Muhando, T. Senjyu, A. Uehara, and T. Funabashi, "Gain-scheduled $H_\infty$ control for WECS via LMI techniques and parametrically dependent feedback Part I: Model development fundamentals," *IEEE Trans. Ind. Electron.*, vol. 58, no. 1, pp. 48–56, Jan. 2011.

[17] F. F. M. El-Sousy, M. Orabi, and H. Godah, "Maximum power point tracking control scheme for grid connected variable speed wind driven self-excited induction generator," *J. Power Electron.*, vol. 6, no. 1, pp. 52–66, Jan. 2006.

[18] E. Ibarra, I. Kortabarria, J. Andreu, I. M. de Alegria, J. L. Martin, and P. Ibanez, "Improvement of the design process of matrix converter platform using the switching state matrix averaging simulation method," *IEEE Trans. Ind. Electron.*, vol. 59, no. 1, pp. 220–234, Jan. 2012.

[19] E. B. Muhando, T. Senjyu, A. Uehara, and T. Funabashi, "Gain-scheduled $H_\infty$ control for WECS via LMI techniques and parametrically dependent feedback Part II: Controller design and implementation," *IEEE Trans. Ind. Electron.*, vol. 58, no. 1, pp. 57–65, Jan. 2011.

[20] R. Pena, J. C. Clare, and G. M. Asher, " A doubly fed induction generator using back-to-back PWM converters and its application to variable-speed wind-energy generation," *Proc. Inst. Elect. Eng.—Elect. Power Appl.*, vol. 143, no. 3, pp. 231–241, May 1996.

[21] A. Luna, F. K. de Araujo Lima, D. Santos, P. Rodriguez, E. H. Watanabe, and S. Arnaltes, "Simplified modelling of a DFIG for transient studies in wind power applications," *IEEE Trans. Ind. Electron.*, vol. 58, no. 1, pp. 9–20, Jan. 2011.

[22] J. P. da Costa, H. Pinheiro, T. Degner, and G. Arnold, "Robust controller for DFIGs of grid-connected wind turbines," *IEEE Trans. Ind. Electron.*, vol. 58, no. 9, pp. 4023–4038, Sep. 2011.

[23] G. Byeon, I.-K. Park, and G. Jang, "Modeling and control of a doubly-fed induction generator (DFIG) wind power generation system for real-time simulations," *J. Elect. Eng. Technol.*, vol. 5, no. 1, pp. 61–69, 2010.

[24] R. Datta and V. T. Ranganathan, "A method of tracking the peak power points for a variable speed wind energy conversion system," *IEEE Trans. Energy Convers.*, vol. 18, no. 1, pp. 163–168, Mar. 2003.

[25] B. Shen, B. Mwinyiwiwa, Y. Zhang, and B.-T. Ooi, "Sensorless maximum power point tracking of wind by DFIG using rotor position phase lock loop," *IEEE Trans. Power Electron.*, vol. 24, no. 4, pp. 942–951, Apr. 2009.

**Kyung-Hyun Kim** was born in 1984. He received the B.S. and M.S. degrees in electrical engineering from Yeungnam University, Gyeongsan, Korea, in 2008 and 2011, respectively.

He is currently with LG Innotek Inc., Ansan, Korea. His research interests include control of power converters, renewable energy systems, and motor drives.

**Tan Luong Van** (S'11) was born in Vietnam in 1979. He received the B.Sc. and M.Sc. degrees in electrical engineering from Ho Chi Minh City University of Technology, Ho Chi Minh City, Vietnam, in 2003 and 2005, respectively. He is currently working toward the Ph.D. degree at Yeungnam University, Gyeongsan, Korea.

In 2003, he was a Lecturer with Ho Chi Minh City Electric Power College, Ho Chi Minh City. His research interests include power converters, machine drives, wind power generation, power quality, and power system.

**Dong-Choon Lee** (S'90–M'95) received the B.S., M.S., and Ph.D. degrees in electrical engineering from Seoul National University, Seoul, Korea, in 1985, 1987, and 1993, respectively.

From 1987 to 1988, he was a Research Engineer with Daewoo Heavy Industry. Since 1994, he has been a Faculty Member with the Department of Electrical Engineering, Yeungnam University, Gyeongsan, Korea. He was a Visiting Scholar with the Power Quality Laboratory, Texas A&M University, College Station, in 1998, with the Electrical Drive Center, University of Nottingham, Nottingham, U.K., in 2001, and with Wisconsin Electric Machines and Power Electronic Consortium, University of Wisconsin, Madison, in 2004. His research interests include ac machine drives, control of power converters, wind power generation, and power quality. He is currently a Publication Editor of the *Journal of Power Electronics* of the Korean Institute of Power Electronics.

**Seung-Ho Song** (S'92–M'95) received the B.S., M.S., and Ph.D. degrees in electrical engineering from Seoul National University, Seoul, Korea, in 1991, 1993, and 1999, respectively.

From 1992 to 1995, he was a Research Engineer with POSCON, where he worked on the development of dc and ac machine drives for steel rolling mill applications. From 2000 to 2006, he was an Assistant Professor with the Division of Electronics and Information, Chonbuk National University, Jeonju, Korea. In 2004, he was also a Visiting Scholar with the Wisconsin Electric Machines and Power Electronic Consortium, University of Wisconsin, Madison. Since 2006, he has been a Faculty Member with the Department of Electrical Engineering, Kwangwoon University, Seoul, Korea, where he is currently a Full Professor. His research interests include electric machine drives and renewable energy conversion.

**Eel-Hwan Kim** (S'89–M'91) received the B.S., M.S., and Ph.D. degrees in electrical engineering from Chung-Ang University, Seoul, Korea, in 1985, 1987, and 1991, respectively.

He was a Visiting Scholar with Ohio State University, Columbus, in 1995 and with the University of Washington, Seattle, in 2004. He is currently a Professor with the Department of Electrical Engineering, Jeju National University, Jeju, Korea. His research activities are in the area of power electronics and control, which includes drive system, renewable energy control applications, and power quality.